Study of $\psi(2S)$ decays to $\gamma p \bar{p}$, $\pi^0 p \bar{p}$, and $\eta p \bar{p}$, and search for $p \bar{p}$ threshold enhancements

J. P. Alexander,[1] D. G. Cassel,[1] S. Das,[1] R. Ehrlich,[1] L. Fields,[1] L. Gibbons,[1] S. W. Gray,[1] D. L. Hartill,[1] B. K. Heltsley,[1] D. L. Kreinick,[1] V. E. Kuznetsov,[1] J. R. Patterson,[1] D. Peterson,[1] D. Riley,[1] A. Ryd,[1] A. J. Sadoff,[1] X. Shi,[1] W. M. Sun,[1] J. Yelton,[2] P. Rubin,[3] N. Lowrey,[4] S. Mehrabyan,[4] M. Selen,[4] J. Wiss,[4] J. Libby,[5] M. Kornicer,[6] R. E. Mitchell,[6] M. R. Shepherd,[6] C. M. Tarbert,[6] D. Besson,[7] T. K. Pedlar,[8] J. Xavier,[8] D. Cronin-Hennessy,[9] J. Hietala,[9] P. Zweber,[9] S. Dobbs,[10] Z. Metreveli,[10] K. K. Seth,[10] A. Tomaradze,[10] T. Xiao,[10] S. Brisbane,[11] L. Martin,[11] A. Powell,[11] P. Spradlin,[11] G. Wilkinson,[11] H. Mendez,[12] J. Y. Ge,[13] D. H. Miller,[13] I. P. J. Shipsey,[13] B. Xin,[13] G. S. Adams,[14] D. Hu,[14] B. Moziak,[14] J. Napolitano,[14] K. M. Ecklund,[15] J. Insler,[16] H. Muramatsu,[16] C. S. Park,[16] L. J. Pearson,[16] E. H. Thorndike,[16] F. Yang,[16] S. Ricciardi,[17] C. Thomas,[11,17] M. Artuso,[18] S. Blusk,[18] R. Mountain,[18] T. Skwarnicki,[18] S. Stone,[18] J. C. Wang,[18] L. M. Zhang,[18] G. Bonvicini,[19] D. Cinabro,[19] A. Lincoln,[19] M. J. Smith,[19] P. Zhou,[19] J. Zhu,[19] P. Naik,[20] J. Rademacker,[20] D. M. Asner,[21,*] K. W. Edwards,[21] K. Randrianarivony,[21] G. Tatishvili,[21,*] R. A. Briere,[22] H. Vogel,[22] P. U. E. Onyisi,[23] and J. L. Rosner[23]

(CLEO Collaboration)

[1]*Cornell University, Ithaca, New York 14853, USA*
[2]*University of Florida, Gainesville, Florida 32611, USA*
[3]*George Mason University, Fairfax, Virginia 22030, USA*
[4]*University of Illinois, Urbana-Champaign, Illinois 61801, USA*
[5]*Indian Institute of Technology Madras, Chennai, Tamil Nadu 600036, India*
[6]*Indiana University, Bloomington, Indiana 47405, USA*
[7]*University of Kansas, Lawrence, Kansas 66045, USA*
[8]*Luther College, Decorah, Iowa 52101, USA*
[9]*University of Minnesota, Minneapolis, Minnesota 55455, USA*
[10]*Northwestern University, Evanston, Illinois 60208, USA*
[11]*University of Oxford, Oxford OX1 3RH, United Kingdom*
[12]*University of Puerto Rico, Mayaguez, Puerto Rico 00681*
[13]*Purdue University, West Lafayette, Indiana 47907, USA*
[14]*Rensselaer Polytechnic Institute, Troy, New York 12180, USA*
[15]*Rice University, Houston, Texas 77005, USA*
[16]*University of Rochester, Rochester, New York 14627, USA*
[17]*STFC Rutherford Appleton Laboratory, Chilton, Didcot, Oxfordshire, OX11 0QX, United Kingdom*
[18]*Syracuse University, Syracuse, New York 13244, USA*
[19]*Wayne State University, Detroit, Michigan 48202, USA*
[20]*University of Bristol, Bristol BS8 1TL, United Kingdom*
[21]*Carleton University, Ottawa, Ontario, Canada K1S 5B6*
[22]*Carnegie Mellon University, Pittsburgh, Pennsylvania 15213, USA*
[23]*University of Chicago, Chicago, Illinois 60637, USA*

The decays of $\psi(2S)$ into $\gamma p \bar{p}$, $\pi^0 p \bar{p}$, and $\eta p \bar{p}$ have been studied with the CLEO-c detector using a sample of 24.5×10^6 $\psi(2S)$ events obtained from $e^+ e^-$ annihilations at $\sqrt{s} = 3686$ MeV. The data show evidence for the excitation of several N^* resonances in $p \pi^0$ and $p \eta$ channels in $\pi^0 p \bar{p}$ and $\eta p \bar{p}$ decays, and f_2 states in $\gamma p \bar{p}$ decay. Branching fractions for decays of $\psi(2S)$ to $\gamma p \bar{p}$, $\pi^0 p \bar{p}$, and $\eta p \bar{p}$ have been determined. No evidence for $p \bar{p}$ threshold enhancements was found in the reactions $\psi(2S) \to X p \bar{p}$, where $X = \gamma$, π^0, η. We do, however, find confirming evidence for a $p \bar{p}$ threshold enhancement in $J/\psi \to \gamma p \bar{p}$ as previously reported by BES.

I. INTRODUCTION

There is long-standing interest in 6-quark dibaryons and 3-quark–3-antiquark "baryonium" states which are permitted in QCD, and may possibly exist. Of particular interest is a possible bound state of a proton and an antiproton. The $p \bar{p}$ state, sometimes called "protonium," was searched for in many experiments, but no credible evidence

---

was found [1,2]. Interest was revived in 2002 by two reports by the Belle Collaboration of threshold enhancements in $M(p\bar{p})$ in the decays $B^{\pm} \rightarrow K^{\pm} p \bar{p}$ [3] and $\bar{B}^0 \rightarrow D^{*0} p \bar{p}$ [4]. These reports were followed by a BES report of threshold enhancement in the decay $J/\psi \rightarrow \gamma p \bar{p}$ [5]. Subsequently, there have been reports of threshold enhancements and studies by Belle in $B^+ \rightarrow \pi^+ p \bar{p}$, $B^0 \rightarrow K^0 p \bar{p}$, and $B^+ \rightarrow K^{*+} p \bar{p}$ [6]; by *BABAR* in $B^+ \rightarrow K^+ p \bar{p}$ [7] and $B^0 \rightarrow p \bar{p} + (\bar{D}^0, \bar{D}^{*0}, D^- \pi^+, \text{or} D^{*-} \pi^+)$ [8]; and most recently by Belle in $B^+ \rightarrow K^+ p \bar{p}$ and $B^+ \rightarrow \pi^+ p \bar{p}$ [9]. Many theoretical explanations, cusp effects, final state interactions, quark fragmentation, and real bound states of quarks and gluons, have been suggested for these threshold enhancements [10].

If the enhancement reported by BES in the decay $J/\psi \rightarrow \gamma p \bar{p}$ [5] is due to a threshold resonance, it is reasonable to expect that evidence for it may be found also in $\psi(2S) \rightarrow \gamma p \bar{p}$. Further insight into its nature may be provided by the study of the reactions $\psi(2S) \rightarrow \pi^0 p \bar{p}$ and $\eta p \bar{p}$.

II. EVENT SELECTION

In this paper we report on studies of these reactions observed in the CLEO-c detector in a data sample of $24.5 \times 10^6 \ \psi(2S)$ events obtained by $e^+ e^-$ annihilations at $\sqrt{s} = 3.686$ GeV at the Cornell Electron Storage Ring, CESR. In addition, we use 20.7 pb^{-1} of off-resonance data taken at $\sqrt{s} = 3.67$ GeV.

The CLEO-c detector, described in detail elsewhere [11], has a solid angle coverage of 93% for charged and neutral particles. The charged particle tracking and identification system operates in a 1.0 T solenoidal magnetic field, and consists of an inner drift chamber, a central drift chamber, and a ring-imaging Cherenkov (RICH) detector. It has a momentum resolution of $\sim 0.6\%$ at momenta of ~ 1 GeV/c. The CsI elecromagnetic calorimeter has a photon energy resolution of $\sim 2.2\%$ for $E_\gamma = 1$ GeV and $\sim 5\%$ at 100 MeV.

Photons and charged particles with $|\cos\theta| < 0.8$ were accepted in the detector, where θ is the polar angle with respect to the incoming positron beam. For the modes involving the direct decays of the $\psi(2S)$, exactly two oppositely charged tracks were required in candidate events. A photon candidate was defined as a shower which does not match a track within 100 mrad, is not in one of the few cells of the electromagnetic calorimeter known to be noisy, has the transverse distribution of energy consistent with an electromagnetic shower, and has an energy more than 30 MeV. For $\gamma p \bar{p}$ the number of showers was required to be ≥ 1, and it was required that the most energetic shower (the signal photon candidate) does not make a π^0 or η with any other shower with a pull mass $< 3\sigma$. For $\pi^0 p \bar{p}$ and $\eta p \bar{p}$ the number of showers was required to be ≥ 2.

To identify charged tracks as protons and antiprotons, the energy loss in the drift chambers (dE/dx) and RICH information was used. For tracks of momentum less than 0.9 GeV/c, only dE/dx information is used. To utilize dE/dx information, for each particle hypothesis, $X = \pi, K, p$, or $\bar{p}$, we calculate $\chi_X^{dE/dx} = [(dE/dx)_{\text{meas}} - (dE/dx)_{\text{pred}}]/\sigma_X$, where $(dE/dx)_{\text{meas}}$ is the measured value of dE/dx, $(dE/dx)_{\text{pred}}$ is the predicted value for hypothesis X, and σ_X is the standard deviation of the measurements for hypothesis X. We cut on both the deviation of the measured dE/dx from a given particle hypothesis, $\chi_X^{dE/dx}$, and the difference in $\chi^{dE/dx}$ between two particle hypotheses, $\Delta\chi_{X,Y}^{dE/dx} \equiv \chi_X^{dE/dx} - \chi_Y^{dE/dx}$. For higher momentum tracks, we use a combined log-likelihood variable. For example, to differentiate between proton and pion we construct

$$\Delta\mathcal{L}_{p,\pi} = (\chi_p^{dE/dx})^2 - (\chi_\pi^{dE/dx})^2 + 2 \times (L_p^{\text{RICH}} - L_\pi^{\text{RICH}}),$$

where $L_{\pi,p}^{\text{RICH}}$ are the log-likelihoods obtained from the RICH subdetector. We use RICH information if the track has $|\cos\theta| < 0.8$ and the track has valid RICH information for at least one hypothesis (pion or proton), and at least three photons consistent with that hypothesis were recorded in the RICH.

We consider three different momentum regions for charged tracks.

(i) $p < 0.9$ GeV/c: In this momentum region only dE/dx information for the tracks is available, and it is required that it be within $3\sigma_p$ of the proton hypothesis, and must be more "protonlike" than "pionlike" or "kaonlike," i.e., $|\chi_p^{dE/dx}| < 3$, $\Delta\chi_{\pi,p} > 0$, and $\Delta\chi_{K,p} > 0$.

(ii) 0.9 GeV/$c < p < 1.15$ GeV/c: In this momentum region, although we are above the threshold for a proton to emit Cherenkov radiation in the RICH, the probability that it will do so is still low. Therefore, if RICH information is available, we require that the track be more protonlike in the combined log-likelihood variable, i.e., $\Delta\mathcal{L}_{p,\pi} < 0$. If RICH information is not available, we again require that $|\chi_p^{dE/dx}| < 3$, and additionally require a 5σ difference between the proton hypothesis and the pion and kaon hypotheses, i.e., $\Delta\chi_{\pi,p} > 5$, and $\Delta\chi_{K,p} > 5$, in order to reduce the number of other particles which pass these cuts.

(iii) $p > 1.15$ GeV/c: In this momentum region, dE/dx alone no longer provides useful information for proton identification. We require that RICH information be available, and that $\Delta\mathcal{L}_{p,\pi} < 0$.

We require one of the charged tracks to be identified as a proton or antiproton and assume the other track to be its antiparticle as required by baryon conservation, and we
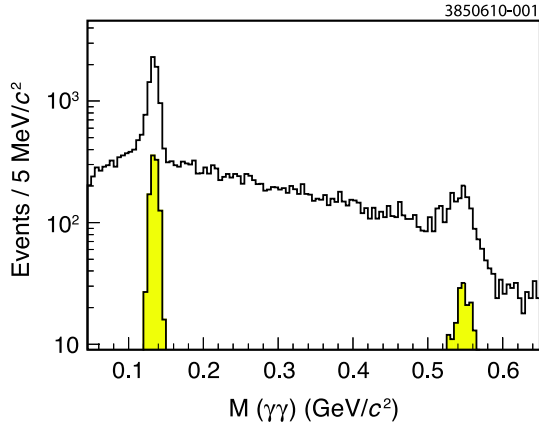
FIG. 1 (color online). Distribution of $M(\gamma\gamma)$ in $\psi(2S) \rightarrow \pi^0(\eta)p\bar{p}$. The unshaded histogram shows the $M(\gamma\gamma)$ distribution before the selection of π^0 and η, and the shaded histogram shows it after the π^0 and η selection described in the text.

require the proton and antiproton to come from a common vertex, with kinematic fit yielding $\chi^2_{p\bar{p}\text{vertex}} < 20$.

Finally, in order to select the events for the channels of interest:

(i) For selection of $\psi(2S) \rightarrow \gamma p\bar{p}$ events we require $\chi^2_{\text{fit}}/\text{degrees of freedom (d.o.f.)} < 5$ for the four-momentum conservation constrained fit to p, $\bar{p}$ and the signal photon candidate.

(ii) For selection of $\psi(2S) \rightarrow \pi^0(\eta)p\bar{p}$ events, we first require that only one $\pi^0(\eta)$ be made by any two photons and the pull mass be within 3σ. Then we require $\chi^2_{\text{fit}}/\text{d.o.f.} < 5$ for the four-momentum conservation constrained fit to p, $\bar{p}$, and $\pi^0(\eta)$. We remove the events corresponding to $\psi(2S) \rightarrow \pi^0(\eta)J/\psi$ by rejecting candidates for which $M(p\bar{p}) = M(J/\psi) \pm 20$ MeV/c^2. Figure 1 shows the distribution of $M(\gamma\gamma)$ before and after the selection of π^0 and η described above.

(iii) For selection of $\psi(2S) \rightarrow \pi^+\pi^-J/\psi$, $J/\psi \rightarrow \gamma p\bar{p}$ events the additional event selection requirements are described in Sec. VIII.

The values of the χ^2 cuts for the fits were selected based on the comparison of the data and the phase space distributions for the individual decays obtained from Monte Carlo (MC) simulations.

III. MONTE CARLO STUDIES

In order to verify the event selection criteria and determine efficiencies, 50 000 phase space MC events were generated for each decay channel analyzed. As an example, for $\psi(2S) \rightarrow \gamma p\bar{p}$ events with $M(p\bar{p}) < 2.85$ GeV/c^2 the contribution of each step of event selection is presented in Table I. The overall phase space efficiency is $(27.7 \pm 0.2)\%$. The corresponding efficiency for $\psi(2S) \rightarrow \pi^0 p\bar{p}$ is $(26.9 \pm 0.2)\%$, and for $\psi(2S) \rightarrow \eta p\bar{p}$ it is $(27.7 \pm 0.2)\%$.

We also use $\psi(2S)$ "generic" MC events with the available statistics of about 5 times data events ($\sim 118 \times 10^6$ events). The generic $\psi(2S)$ MC sample is generated using the available branching fractions for the $\psi(2S)$, χ_{cJ}, J/ψ, and η_c decays, with unmeasured decay modes simulated by JETSET [12]. We have tested the event selection using a generic MC sample. We apply the same event selection to these MC events, extract the different branching fractions, and compare them to the branching fractions which were input in creating the generic MC sample. The agreement between the input and output branching fractions for $\psi(2S) \rightarrow \gamma p\bar{p}$, $\pi^0 p\bar{p}$, and $\eta p\bar{p}$ is found to be within $(2.4 \pm 3.9)\%$, $(1.0 \pm 1.0)\%$, and $(3.0 \pm 4.0)\%$, respectively.

IV. OVERVIEW OF $\psi(2S)$ DECAYS

Figure 2 shows Dalitz plots for the data for the three decays. All three Dalitz plots show event populations which are far from uniform, as would be expected for pure phase space decays, and suggest contribution by intermediate excited nucleon states, N^*, and mesons. Since the branching fractions for N^* decays to $N\pi$ and $N\eta$ are generally much larger than those for decays to $N\gamma$, we expect excitation of N^* states in $\psi(2S) \rightarrow \pi^0 p\bar{p}$ and $\psi(2S) \rightarrow \eta p\bar{p}$. Similarly, we expect excitation of intermediate meson states which decay into $p\bar{p}$, f_J states in $\psi(2S) \rightarrow \gamma p\bar{p}$ and $\eta p\bar{p}$, and a_J states in $\psi(2S) \rightarrow \pi^0 p\bar{p}$.

A caveat about the intermediate states is in order. The intermediate N^* and $f_{0,2}$ states which we use in our analysis tend to have masses ≥ 1.5 GeV/c^2. Unfortunately, the existence of most high mass N^* resonances is either uncertain or poorly established, and their masses and widths

TABLE I. Efficiencies of the individual event selection criteria for the decay $\psi(2S) \rightarrow \gamma p\bar{p}$ based on phase space MC simulation.

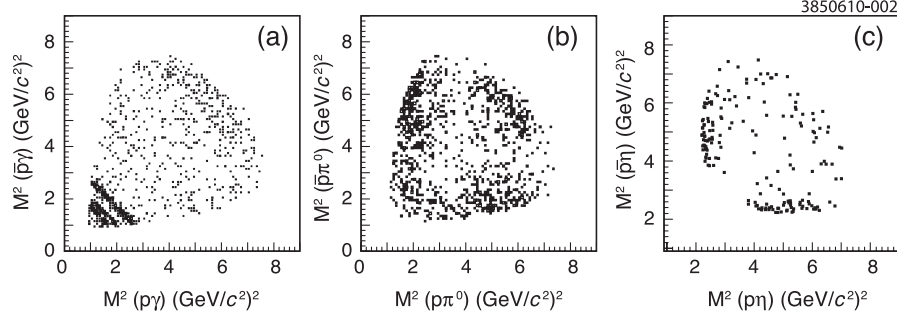| Selection requirement	Efficiency (%)
Charged track and photon selection $N_{ch} = 2$, net charge $= 0$, $N_\gamma \geq 1$	74.5
Signal photon does not make π^0 with any other shower	97.0
Vertex fit, constrained fit $\chi^2_{\text{vertex}} < 20$, $\chi^2_{\text{fit}} < 5$	84.3
Proton-antiproton identification	98.2
$M(p\bar{p}) < 2.85$ GeV/c^2	64.3
All p, $\bar{p}$ and most energetic photon are in the barrel ($|\cos\theta| < 0.8$)	72.0
Total	27.7

FIG. 2. (a) Dalitz plots for the data: (a) $M^2(p\gamma)$ versus $M^2(\bar{p}\gamma)$ for $\psi(2S) \to \gamma p \bar{p}$; (b) $M^2(p\pi^0)$ versus $M^2(\bar{p}\pi^0)$ for $\psi(2S) \to \pi^0 p \bar{p}$; (c) $M^2(p\eta)$ versus $M^2(\bar{p}\eta)$ for $\psi(2S) \to \eta p \bar{p}$.

have large uncertainties, so much so that the 2008 Particle Data review (PDG08) [13] omits many of them from its summary table. Similar uncertainties exist for meson states with masses ≥ 1.5 GeV/c^2. Therefore our identification of an observed resonance with a known resonance is necessarily tentative.

Our data lack the statistics to make a full partial wave analysis. Instead, we analyze the projections of the Dalitz plots of invariant mass distributions for $M(p(\gamma, \pi^0, \eta))$ and $M(p\bar{p})$. Throughout this paper, charge conjugate states and their contributions are implied.

We fit the invariant mass distributions with contributions from phase space and the minimum number of resonances required to obtain good fits. The resonances are parametrized in terms of relativistic Breit-Wigner functions with mass dependent widths and include the Blatt-Weisskopf penetration factors ([13], see p. 772). We note that peak positions and widths in the relativistic fits can be substantially different from those for the simple Breit-Wigner function, particularly for large widths and proximity to thresholds [13].

In order to take proper account of intermediate states and possible reflections in the Dalitz plots we analyze the data in the full range of $p\bar{p}$ invariant mass, from threshold to 3.6 GeV/c^2. In this important respect the present analysis differs from the BES analyses [5,14,15].

In Secs. V, VI, and VII we discuss the decays $\psi(2S) \to \gamma p \bar{p}$, $\pi^0 p \bar{p}$, and $\eta p \bar{p}$, respectively. In Sec. VIII we present the results of the analysis of our limited statistics sample of $J/\psi \to \gamma p \bar{p}$ events.

V. THE DECAY $\psi(2S) \to \gamma p \bar{p}$

For the search for a threshold enhancement in $\psi(2S) \to \gamma p \bar{p}$, and for the measurement of the inclusive branching fraction $\mathcal{B}(\psi(2S) \to \gamma p \bar{p})$, we limit ourselves to $M(p\bar{p}) < 2.85$ GeV/c^2, below the η_c mass. As a check on our analysis technique, we use our data for $M(p\bar{p}) > 3.15$ GeV/c^2 to calculate the $\mathcal{B}(\chi_{cJ} \to p\bar{p})$ branching fractions and compare them to recent measurements.

In Fig. 3 we show the χ^2 distributions for the data and the phase space MC events for vertex fit and four-momentum conservation constrained fit to the proton,

antiproton, and most energetic shower in the event. All other selection criteria have been applied. Comparison of these distributions suggests the cut values $\chi^2_{p\bar{p}\text{vertex}} < 20$ and $\chi^2_{\text{fit}} < 20$.

In Fig. 4 we compare E/pc distributions for protons and antiprotons in data and the phase space $\psi(2S) \to \gamma p \bar{p}$ MC simulation, where E is the energy determined from the calorimeter and p is the momentum determined from track reconstruction. The distributions of protons and antiprotons are different, because antiprotons annihilate in the
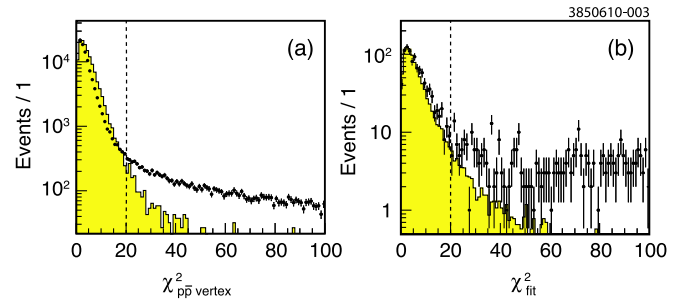

FIG. 3 (color online). Distributions of the χ^2 of four-momentum conservation constrained fits for $\psi(2S) \to \gamma p \bar{p}$: (a) χ^2 of vertex fit, (b) χ^2 of the four-momentum conservation fit. Points correspond to the data and the shaded histograms correspond to the phase space MC simulation. Dashed lines indicate the cut values used.
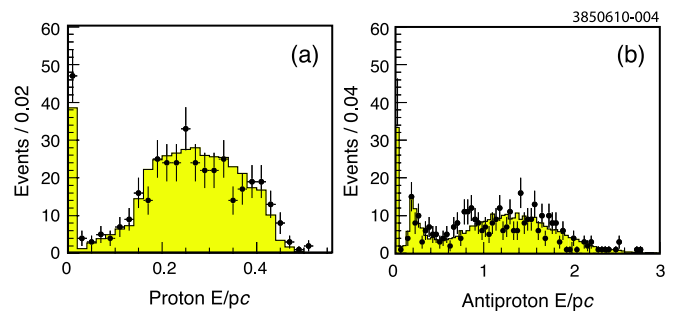

FIG. 4 (color online). Distributions of E/pc for $\psi(2S) \to \gamma p \bar{p}$ for $M(p\bar{p}) < 2.85$ GeV/c^2: (a) protons, (b) antiprotons. Because of annihilations E/p for antiprotons extends over a much larger range than for protons. Points correspond to the data and the shaded histograms to the phase space MC simulation.
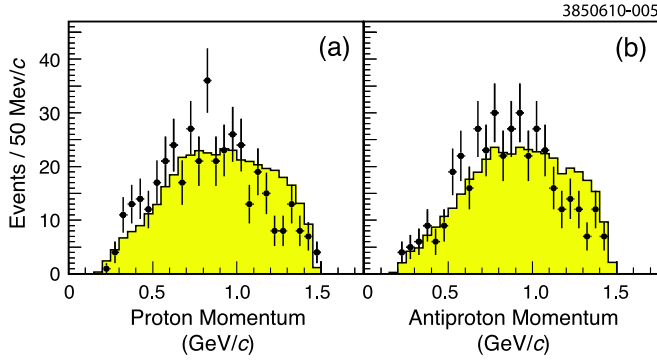
FIG. 5 (color online). Distributions of the momenta of charged particles for $\psi(2S) \to \gamma p\bar{p}$: (a) protons, (b) antiprotons. Points correspond to the data and the shaded histograms to the phase space MC simulation.

material of the electromagnetic calorimeter. However, for both protons and antiprotons, the data and the phase space MC distributions show good agreement.

In Fig. 5 proton and antiproton momentum distributions for the data and the phase space $\psi(2S) \to \gamma p\bar{p}$ MC simulation are shown. The agreement between MC simulation and data momentum distributions is not good, and may indicate the effect of intermediate resonances.

In Fig. 6 we present the $M(p\bar{p})$ invariant mass distributions for the data and the $\psi(2S)$ generic MC simulation, which includes the excitation of χ_{cJ} and η_c, but not the initial state radiation generated J/ψ. All event selection criteria have been applied. The generic MC events are normalized to the number of $\psi(2S)$ events in the data for a qualitative comparison.

In Fig. 6 we note that there is an excess of events in the data over the generic MC simulation in the region $M(p\bar{p}) < 2.3$ GeV/c^2. The generic MC simulation has no input for possible resonances in this mass region.

The excitation of the χ_{cJ} states, shown in Fig. 6, gives us an opportunity to further test the appropriateness of our event selection.

To extract χ_{cJ} branching ratios we fit the photon energy E_γ distribution shown in Fig. 7 with Breit-Wigner functions convolved with Crystal Ball line shape [16], and a second-order polynomial background. The fit results
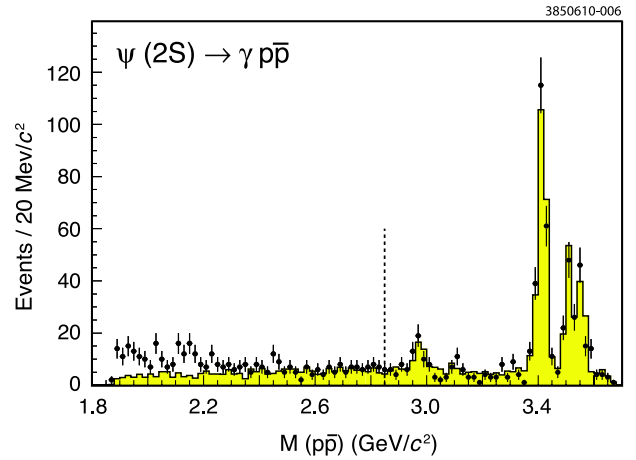

FIG. 6 (color online). Distribution of $M(p\bar{p})$ for $\psi(2S) \to \gamma p\bar{p}$. All event selection criteria have been applied. The points represent data and the shaded histogram is the generic MC distribution, which is normalized to the 24.5×10^6 $\psi(2S)$ events in data. The dashed line indicates the $M(p\bar{p}) = 2.85$ GeV/c^2 limit of the range used for $\psi(2S) \to \gamma p\bar{p}$ branching fraction calculations.
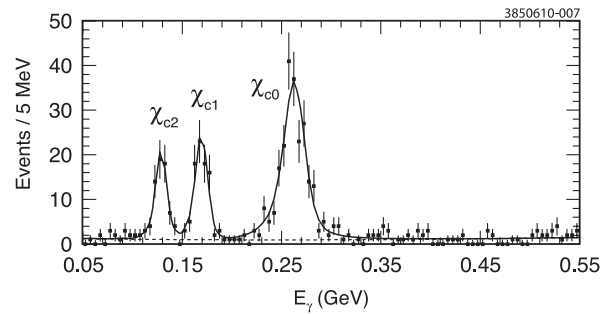

FIG. 7. Fit of the photon energy distribution for $\psi(2S) \to \gamma p\bar{p}$. Events in the figure are the same as in Fig. 6. The fit has $\chi^2/\text{d.o.f.} = 100/98$.

for photon energies agree with those expected for the χ_{cJ} resonances within ± 2 MeV. As seen in Table II, our calculated values of $\mathcal{B}(\chi_{cJ} \to p\bar{p})$ agree within errors with both the results of a recent CLEO measurement [17], which use the same data, and PDG08 [13].

TABLE II. Results for $\mathcal{B}(\chi_{cJ} \to p\bar{p})$ for χ_{cJ} states. The PDG08 values for $\mathcal{B}(\psi(2S) \to \gamma\chi_{cJ})$ have been used to obtain the results for $\mathcal{B}(\chi_{cJ} \to p\bar{p})$.

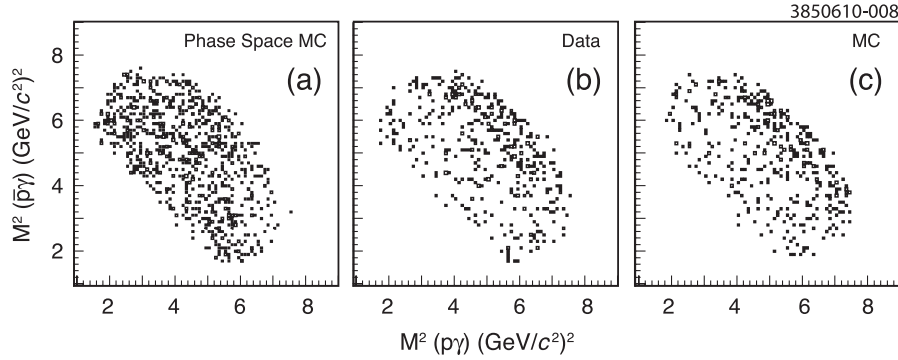|	χ_{c0}	χ_{c1}	χ_{c2}
Mass (MeV/c^2)	3412.8 ± 1.0	3512.5 ± 0.4	3555.0 ± 1.0
N (events)	236.0 ± 18.4	79.0 ± 10.7	62.5 ± 9.8
Efficiency in %	39.5	41.4	37.9
$\mathcal{B}(\psi(2S) \to \gamma\chi_{cJ}) \times \mathcal{B}(\chi_{cJ} \to p\bar{p}) \times 10^6$	22.0 ± 1.7	7.05 ± 0.96	6.07 ± 0.95
$\mathcal{B}(\chi_{cJ} \to p\bar{p}) \times 10^5$ (this analysis)	23.4 ± 2.1	8.0 ± 1.1	7.3 ± 1.2
$\mathcal{B}(\chi_{cJ} \to p\bar{p}) \times 10^5$ (CLEO [17])	$25.7 \pm 1.5 \pm 2.0$	$9.0 \pm 0.8 \pm 0.6$	$7.7 \pm 0.8 \pm 0.6$
$\mathcal{B}(\chi_{cJ} \to p\bar{p}) \times 10^5$ (PDG08 [13])	21.4 ± 1.9	6.6 ± 0.5	6.7 ± 0.5

FIG. 8. Dalitz plots of $M^2(p\gamma)$ versus $M^2(\bar{p}\gamma)$ for $\psi(2S) \to \gamma p\bar{p}$: (a) the phase space MC simulation; (b) the data; (c) the sum of three MC plots for $f_2(1950)$, $f_2(2150)$, and phase space.
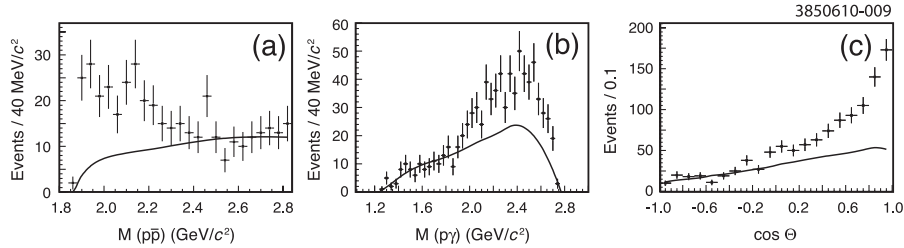

FIG. 9. Distributions in data (points) compared to the phase space MC distributions (solid lines): (a) the $M(p\bar{p})$ invariant mass distributions; (b) the $M(p\gamma)$ distributions; (c) the $\cos\Theta$ distributions. Phase space normalization is arbitrary in all plots.

These measurements are intended as checks on the analysis technique only and not as new measurements, and no systematic errors are included.

In order to explore the intermediate state resonances which are excited in the reaction $\psi(2S) \to \gamma p\bar{p}$ we study several presentations of the data. These include the $p\gamma$ versus $\bar{p}\gamma$ Dalitz plot, the $M(p\bar{p})$ and $M(p\gamma)$ projections, and the distributions of $\cos\Theta$, where Θ is the angle between the proton and antiproton in the rest frame of the photon-proton system.

The three panels in Fig. 8 show $M^2(p\gamma)$ versus $M^2(\bar{p}\gamma)$ Dalitz plots, respectively, for phase space MC simulation, data, and MC simulation with the intermediate resonances as described below. Figure 9 shows phase space MC distributions superimposed on the data for $M(p\bar{p})$, $M(p\gamma, \bar{p}\gamma)$, and $\cos\Theta$. (In the last two plots events have been included for both $p\gamma$ and $\bar{p}\gamma$, resulting in double counting.)

In the distributions shown in Figs. 8 and 9, it is clear that pure phase space distributions fail to describe the data.

Significant contributions by intermediate states are required. We have made MC studies of the contributions that various known scalar and tensor meson resonances would make to these distributions. We find that the best candidates are $f_2(1950)$ and $f_2(2150)$ with parameters given in PDG08. We determine MC shapes of the contributions that $f_2(1950)$, $f_2(2150)$, and phase space make to the distributions for $M(p\bar{p})$, $M(p\gamma)$, and $\cos\Theta$, and determine their relative magnitudes by fitting the data distributions. Using the PDG08 [13] values for masses and widths for the two resonances, the best fit is obtained with relative fractions listed in Table III. The corresponding MC-determined efficiencies, which are found to be insensitive to the uncertainties in masses and widths of the resonances, are also listed in the table. The overall efficiency of the admixture of the resonances and phase space is

$$\langle\epsilon\rangle = 0.336 \pm 0.008. \tag{1}$$

As shown in Fig. 10 good fits to all three distributions are obtained with the above admixtures, their respective

TABLE III. Fractions and efficiencies for the intermediate resonances and the phase space contribution for the best fits for the reaction $\psi(2S) \to \gamma p\bar{p}$.

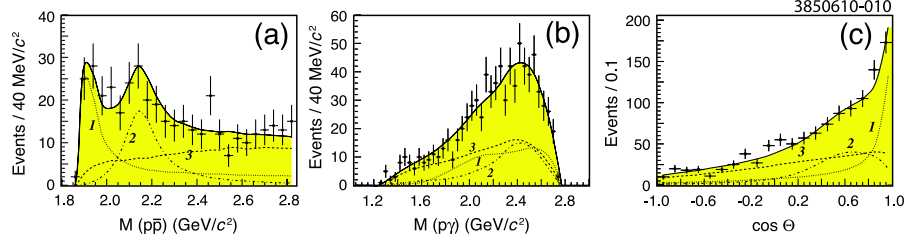| State	M (MeV/c^2)	Γ (MeV/c^2)	Fraction (%)	ϵ
$f_2(1950)$	1944 ± 12	472 ± 18	32 ± 5	0.375
$f_2(2150)$	2156 ± 11	167 ± 30	21 ± 5	0.410
Phase space			47 ± 6	0.277

FIG. 10 (color online). Distributions in data (points) compared with the sum of the MC distributions in the proportions given in Table III (solid lines): (a) the $M(p\bar{p})$ invariant mass distributions; (b) the $M(p\gamma)$ distributions; (c) the $\cos\Theta$ distributions. The individual contributions are $f_2(1950)$ shown with the dotted line marked 1, $f_2(2150)$ shown with the dash-dotted line marked 2, and phase space shown with the dashed line marked 3.

$\chi^2/$d.o.f. being 15/24 for $M(p\bar{p})$, 33/35 for $M(p\gamma)$, and 23/20 for $\cos\Theta$. The resulting Dalitz plot, shown in Fig. 8(c), is also in good qualitative agreement with that for the data. No evidence is found in the data for a narrow resonance R with $\Gamma_R < 40$ MeV/c^2 anywhere in the region $M(p\bar{p}) = 2200$–2800 MeV/c^2. The 90% confidence level upper limit is $\mathcal{B}(\psi(2S) \to \gamma R) \times \mathcal{B}(R \to p\bar{p}) < 2 \times 10^{-6}$.

A. Determination of $\mathcal{B}(\psi(2S) \to \gamma p\bar{p})$

In the region $M(p\bar{p}) < 2.85$ GeV/c^2, we obtain $N = 407 \pm 20$ $\psi(2S) \to \gamma p\bar{p}$ candidate events. We evaluate the background due to $\psi(2S) \to \pi^0 p\bar{p}$, in which one photon from the π^0 decay is lost, as $N_{\text{bkg}}(\pi^0) = 38 \pm 2$. In addition, by analyzing the continuum data at $\sqrt{s} = 3.76$ GeV we determine that the luminosity-normalized continuum background contribution is $N_{\text{cont}} = 26 \pm 8$ counts. With the relative contributions of $f_2(1950)$, $f_2(2150)$, and phase space as in Table III, and the effective overall efficiency [Eq. (1)], we get

$$\mathcal{B}(\psi(2S) \to p\bar{p}\gamma) = \frac{N - N_{\text{bkg}} - N_{\text{cont}}}{\langle \epsilon \rangle \times N_{\psi(2S)}}$$

$$= (4.18 \pm 0.26(\text{stat})) \times 10^{-5}. \quad (2)$$

The individual product branching fractions are

$$\mathcal{B}(\psi(2S) \to \gamma f_2(1950)) \times \mathcal{B}(f_2(1950) \to p\bar{p})$$

$$= (1.2 \pm 0.2(\text{stat})) \times 10^{-5}, \quad (3)$$

$$\mathcal{B}(\psi(2S) \to \gamma f_2(2150)) \times \mathcal{B}(f_2(2150) \to p\bar{p})$$

$$= (0.72 \pm 0.18(\text{stat})) \times 10^{-5}. \quad (4)$$

Estimates of systematic errors are provided in Sec. IX.

Our result for $\mathcal{B}(\psi(2S) \to \gamma p\bar{p})$ differs by 2σ from the PDG08 result based on the BES measurement [14], $\mathcal{B}(\psi(2S) \to \gamma p\bar{p}) = (2.9 \pm 0.6) \times 10^{-5}$, in which no account of intermediate resonances was taken. The results in Eqs. (3) and (4) represent the first measurements of these product branching fractions.

B. Search for threshold enhancement in $\psi(2S) \to \gamma p\bar{p}$

Figure 10(a) shows that a good fit to the $M(p\bar{p})$ spectrum is obtained with the sum of contributions from $f_2(1950)$, $f_2(2150)$, and phase space, with $\chi^2/$d.o.f. $= 15/24$. No threshold resonance seems to be needed. However, to reach a quantitative conclusion we study in detail the $p\bar{p}$ threshold region, $\Delta M = M(p\bar{p}) - 2m_p = 0$–300 MeV/$c^2$. To do so, we evaluate the contributions of the f_2 resonances and phase space in this region, and determine the efficiency for $\psi(2S) \to \gamma R_{\text{thr}}$, $R_{\text{thr}} \to p\bar{p}$ in this region. The results are shown in Fig. 11.

The $\Delta M = M(p\bar{p}) - 2m_p$ event distribution is shown in Fig. 12. A visual inspection of the distributions shows that there is no evidence for a statistically significant enhancement at the threshold, $\Delta M = 0$. In fact, a straight line fit to the data gives $\chi^2/$d.o.f. $= 52/58$. However, we must consider the contributions due to the f_2 resonances and phase space as has been determined in Table III, and as shown in Fig. 11(b), and the efficiency $\langle \epsilon \rangle = 55.8\%$ in the threshold region. Figure 12 shows the best fit obtained using these contributions plus a Breit-Wigner threshold resonance with the parameters obtained by BES [5], namely, $M(p\bar{p}) = 1859$ MeV/c^2, and $\Gamma = 20$ MeV/c^2. The fit has $\chi^2/$d.o.f. $= 53/58$, and includes the best fit threshold resonance R_{thr} with 9^{+10}_{-9} counts. This leads to
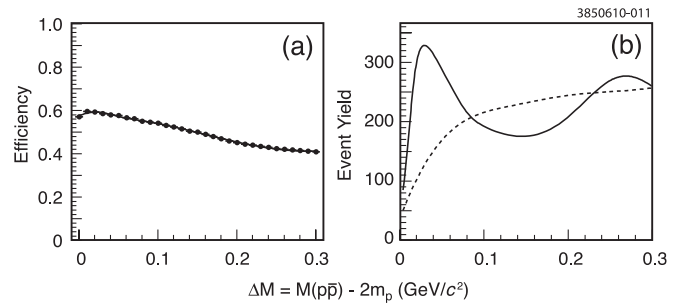

FIG. 11. (a) MC-determined efficiency as a function of $\Delta M = M(p\bar{p}) - 2m_p$ for $\psi(2S) \to \gamma R_{\text{thr}}$, $R_{\text{thr}} \to p\bar{p}$. (b) The solid curve is the shape of the ΔM distribution from MC simulation for the admixtures shown in Table III, and the dashed curve is the shape of the ΔM distribution from MC simulation for phase space alone. Relative normalizations are arbitrary.
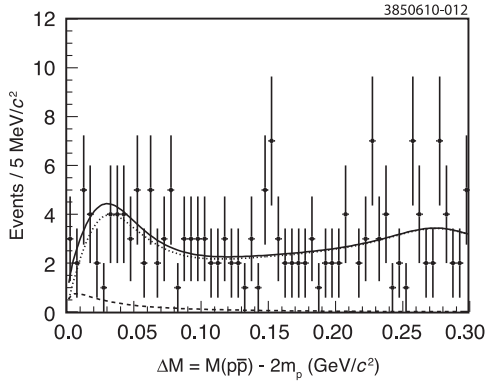
FIG. 12. Fits of the $\Delta M \equiv M(p\bar{p}) - 2m_p$ distribution for $\psi(2S) \to \gamma p \bar{p}$ decay. The dotted line is the sum of the resonance and phase space contributions according to Table III, and the dashed line shows the fitted threshold resonance contribution. The solid line is the sum of all contributions.

$$\mathcal{B}(\psi(2S) \to \gamma R_{\text{thr}}) \times \mathcal{B}(R_{\text{thr}} \to p\bar{p}) = \frac{N_R}{\epsilon N_{\psi(2S)}}$$

$$= (0.66^{+0.73}_{-0.66}) \times 10^{-6} \quad \text{or} \quad < 1.6 \times 10^{-6}, \qquad 90\% \text{CL}, \tag{5}$$

where CL means confidence level. This is more than a factor 3 more restrictive than the current best limit [14].

VI. THE DECAY $\psi(2S) \to \pi^0 p \bar{p}$

Our analysis of $\psi(2S) \to \pi^0 p \bar{p}$ follows the same steps as described in Sec. IV for $\psi(2S) \to \gamma p \bar{p}$. Figure 13 shows

the three Dalitz plots, respectively, for (a) phase space MC simulation, (b) data, and (c) MC simulation with the resonances described below. The phase space and data Dalitz plots differ dramatically, and the MC plot with the resonances described below is in impressive agreement with the data. Figure 14 shows the projected distributions for $M(p\pi^0)$, $M(p\bar{p})$, and $\cos\Theta$, the polar angle of p in the rest frame of $\pi^0 p$. It is clear that the pure phase space distributions do not reproduce the data in either the Dalitz plots or the projected distributions. Figure 15 shows the same three distributions with good quality fits based on resonance shapes determined from MC simulations, as described below.

The N^* intermediate states in $\psi(2S) \to \pi^0 p \bar{p}$ are most clearly visible in the $M(p\pi^0)$ distribution of Fig. 14(a), with enhancements near $M(p\pi^0) \approx 1400 \text{ MeV}/c^2$ and $M(p\pi^0) \approx 2300 \text{ MeV}/c^2$. Similarly, the meson intermediate states are most clearly visible in the $M(p\bar{p})$ distribution of Fig. 14(b), with enhancements near $M(p\bar{p}) \approx 2100 \text{ MeV}/c^2$ and $M(p\bar{p}) \approx 2900 \text{ MeV}/c^2$. The enhancement at $M(p\pi^0) \approx 1400 \text{ MeV}/c^2$ can be identified with the well known $N^*(1440)$, which we call N_1^*, and the enhancement at $M(p\bar{p}) \approx 2100 \text{ MeV}/c^2$, which we call R_1, can be identified with the known resonance $f_0(2100)$ [13]. The large enhancements in $M(p\pi^0)$ at 2300 MeV/c^2, which we call N_2^*, and in $M(p\bar{p})$ at 2900 MeV/c^2, which we call R_2, cannot be identified with known N^* and $f_{0,2}$ resonances, and we have to take an empirical approach for them.

Because the mass and width of $f_0(2100)$ are well defined, in all subsequent analysis we keep them fixed to their
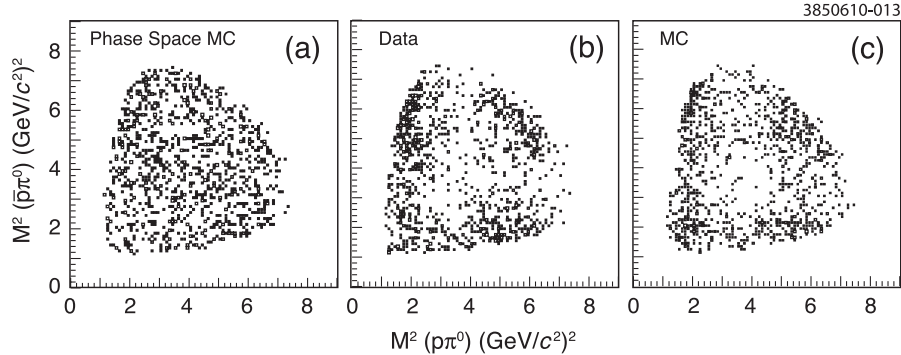

FIG. 13. Dalitz plots of $M^2(p\pi^0)$ versus $M^2(\bar{p}\pi^0)$ for the channel $\psi(2S) \to \pi^0 p \bar{p}$: (a) the phase space MC simulation; (b) the data; (c) the sum of four MC plots for $R_1(2100)$, $R_2(2900)$, $N_1^*(1440)$, and $N_2^*(2300)$.
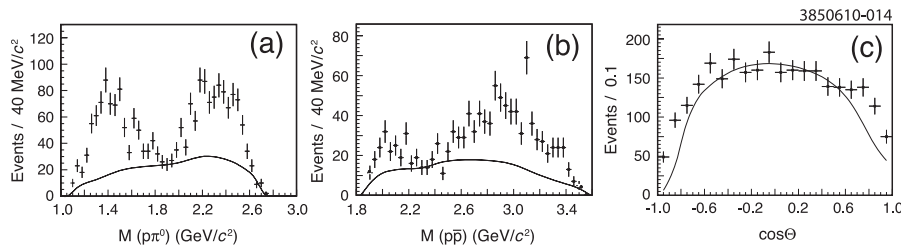

FIG. 14. Distributions in data (points) compared to the phase space MC distributions: (a) the $M(p\pi^0)$ distributions, (b) the $M(p\bar{p})$ invariant mass distributions, (c) the $\cos\Theta$ distributions. Normalization is arbitrary in all plots.
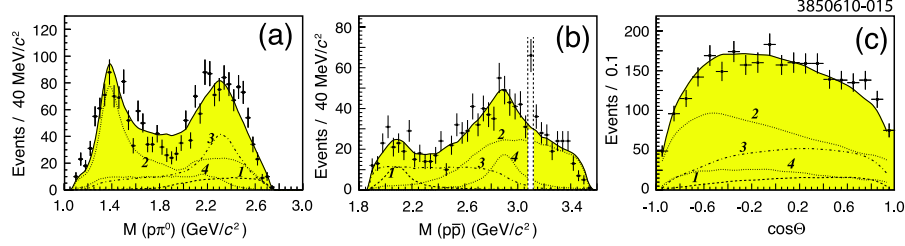
FIG. 15 (color online). Distributions in data (points) compared to the sum of the MC distributions in the proportions given in Table IV (solid lines): (a) the $M(p\pi^0)$ distributions; (b) the $M(p\bar{p})$ distributions; (c) the $\cos\Theta$ distributions. The individual contributions are $R_1(2100)$ shown with the dashed line marked 1, $N_1^*(1440)$ shown with the dotted line marked 2, $N_2^*(2300)$ shown with the dash-dotted line marked 3, $R_2(2900)$ shown with the dotted line marked 4.

PDG08 values. To determine the optimum values for the masses and widths of the N_1^*, N_2^*, and R_2 resonances, the following procedure was used.

Because the Dalitz plot projections contain reflections, the projections cannot be fitted with simple Breit-Wigner resonances. Instead, MC distributions have to be generated for individual resonances with assumed masses and widths, and their optimum values have to be determined by fitting the data distributions with the MC generated distributions. Our procedure takes account of reflections, but does not include taking account of any possible interferences between resonances.

We first fit the $M(p\pi^0)$ distribution with only N_1^* and N_2^* resonances and determine the best fit values for their masses and widths by iterating each in 5 MeV/c^2 steps. We then fit the $M(p\bar{p})$ distribution with just the above N_1^* and N_2^* resonances. We find that the $M(p\bar{p})$ distribution is fitted poorly, with χ^2/d.o.f. $= 65/37$, and the enhancements at $M(p\bar{p}) \approx 2100$ MeV/c^2 and $M(p\bar{p}) \approx 2900$ MeV/c^2 are not reproduced. We then explicitly introduce fixed parameter $R_1(2100)$, and R_2 on whose parameters we iterate to find their best values. As expected, the fit to the $M(p\bar{p})$ distribution is improved, with χ^2/d.o.f. $= 44/33$. We go back to the $M(p\pi^0)$ distribution to determine the effect of including R_1 and R_2. It is found that their contribution is structureless in the $M(p\pi^0)$ distribution, and it does not affect the best fit parameters of N_1^* and N_2^*.

In Table IV final resonance parameters of N_1^*, N_2^*, R_1, and R_2 are listed. The errors in the masses and widths are those which change the likelihood of fits by two units.

The efficiencies are as determined by MC simulations. The relative fractions are determined by the final fit to the $M(p\bar{p})$ distribution.

The fits obtained for $M(p\pi^0)$, $M(p\bar{p})$, and $\cos\Theta$ distributions with the final set of parameters for all four resonances are shown in Figs. 15(a)–15(c). The individual resonance contributions are shown with dotted and dashed lines. The corresponding composite Dalitz plot is shown in Fig. 13(c). It agrees very well with that for data in Fig. 13(b). No evidence for a $p\bar{p}$ threshold enhancement is observed in the $M(p\bar{p})$ distribution of Fig. 15(b).

BES reported the result for $\psi(2S) \to \pi^0 p\bar{p}$ using its sample of 14×10^6 $\psi(2S)$ events [15]. Since the number of events was almost a factor of 2 smaller than in the present investigation, BES was not able to reach any conclusions about intermediate states other than to note that there was "indication of some enhancement around 2 GeV/c^2."

Determination of $\mathcal{B}(\psi(2S) \to \pi^0 p\bar{p})$

We consider all events in the $M(p\bar{p})$ spectrum for $M(p\bar{p}) < 3.6$ GeV/c^2 [Fig. 15(b)] for determination of the branching fraction $\mathcal{B}(\psi(2S) \to \pi^0 p\bar{p})$, except those with $M(p\bar{p}) = 3.097 \pm 0.020$ GeV/c^2, which could come from J/ψ production.

We obtain $N = 1063 \pm 33$ $\psi(2S) \to \pi^0 p\bar{p}$ candidate events. Using our branching fraction of $\mathcal{B}(\psi(2S) \to \gamma p\bar{p}) = (4.18 \pm 0.26) \times 10^{-5}$, and the efficiency determined in Eq. (1), we estimate $N_{\text{bkg}} = 15 \pm 1$ background counts due to misidentified $\gamma p\bar{p}$ events.

We estimate the nonresonant contribution of $\pi^0 p\bar{p}$ production by using the data taken at the off-$\psi(2S)$ resonance energy of $\sqrt{s} = 3.67$ GeV. It leads to a luminosity-normalized nonresonant contribution in our data, $N_{\text{cont}} = 105 \pm 16$.

The efficiencies determined from the $N_1^*(1440)$, $N_2^*(2300)$, $R_1(2100)$, and $R_2(2900)$ MC simulations are 24.1%, 27.6%, 27.5%, and 24.1%, respectively. The overall efficiency of the admixture of the resonances is $\langle \epsilon \rangle = (25.4 \pm 0.2)\%$.

TABLE IV. Fractions and efficiencies for the intermediate resonances for the reaction $\psi(2S) \to \pi^0 p\bar{p}$.

Resonance	M (MeV/c^2)	Γ (MeV/c^2)	Fraction (%)	ϵ
$N_1^*(1440)$	1400 ± 25	220 ± 20	50 ± 4	0.241
$N_2^*(2300)$	2300 ± 25	300 ± 30	28 ± 4	0.276
$R_1(2100)$	2103 ± 8	209 ± 19	8 ± 3	0.275
$R_2(2900)$	2900 ± 20	250 ± 25	24 ± 4	0.241

This yields a branching fraction of

$$\mathcal{B}(\psi(2S) \to p\bar{p}\pi^0) = \frac{N - N_{\text{bkg}} - N_{\text{cont}}}{\langle \epsilon \rangle \times N_{\psi(2S)} \times \mathcal{B}(\pi^0 \to \gamma\gamma)}$$

$$= (1.54 \pm 0.06(\text{stat})) \times 10^{-4}. \tag{6}$$

This result is in agreement with the PDG08 [13] value of $(1.33 \pm 0.17) \times 10^{-4}$, and has a factor 3 smaller error.

We can also determine the product branching fractions for the $N_1^*(1440)$, $N_2^*(2300)$, $R_1(2100)$, and $R_2(2900)$ resonances by taking account of their respective fractions and efficiencies given in Table IV. The resulting product branching fractions are

$$\mathcal{B}(\psi(2S) \to \bar{p}N_1^*(1440)) \times \mathcal{B}(N_1^*(1440) \to p\pi^0)$$

$$= (8.1 \pm 0.7(\text{stat})) \times 10^{-5}, \tag{7}$$

$$\mathcal{B}(\psi(2S) \to \bar{p}N_2^*(2320)) \times \mathcal{B}(N_2^*(2320) \to p\pi^0)$$

$$= (4.0 \pm 0.6(\text{stat})) \times 10^{-5}, \tag{8}$$

$$\mathcal{B}(\psi(2S) \to \pi^0 R_1(2100)) \times \mathcal{B}(R_1(2100) \to p\bar{p})$$

$$= (1.1 \pm 0.4(\text{stat})) \times 10^{-5}, \tag{9}$$

$$\mathcal{B}(\psi(2S) \to \pi^0 R_2(2900)) \times \mathcal{B}(R_2(2900) \to p\bar{p})$$

$$= (2.3 \pm 0.7(\text{stat})) \times 10^{-5}. \tag{10}$$

These are the first determinations of these product branching fractions. Estimates of systematic errors are provided in Sec. IX.

VII. THE DECAY $\psi(2S) \to \eta p\bar{p}$

As shown in Fig. 1, the yield of $\eta p\bar{p}$ (184 counts) is nearly a factor of 6 smaller than for $\pi^0 p\bar{p}$ (1063 counts). Dalitz plots of $M^2(p\eta)$ versus $M^2(\bar{p}\eta)$ are shown in Fig. 16, (a) for pure phase space, (b) for the data, and (c) for resonances described below. As in the $\psi(2S) \to \pi^0 p\bar{p}$ case, it is seen that the Dalitz plot for the data [Fig. 16(b)] is completely different from the uniformly populated Dalitz plot for phase space MC simulation [Fig. 16(a)]. The data are clearly dominated by the contribution of intermediate states. As shown in Fig. 16(c) the sum of MC simulated contributions of resonances described below reproduces the data very well.

The projected distributions for (a) $M(p\eta)$, (b) $M(p\bar{p})$, and (c) $\cos\Theta$, where Θ is the polar angle of the p in the rest frame of ηp, are shown in Fig. 17, together with MC generated distributions for phase space. As expected, the phase space distributions do not reproduce the data distributions.
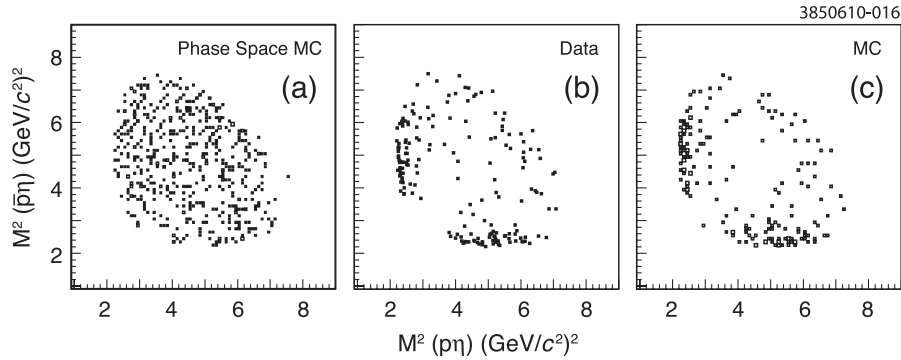

FIG. 16. Dalitz plots of $M^2(p\eta)$ versus $M^2(\bar{p}\eta)$ for the channel $\psi(2S) \to \eta p\bar{p}$: (a) the phase space MC simulation; (b) the data; (c) the sum of two MC plots for $R_1(2100)$ (20%), and $N^*(1535)$ (80%).
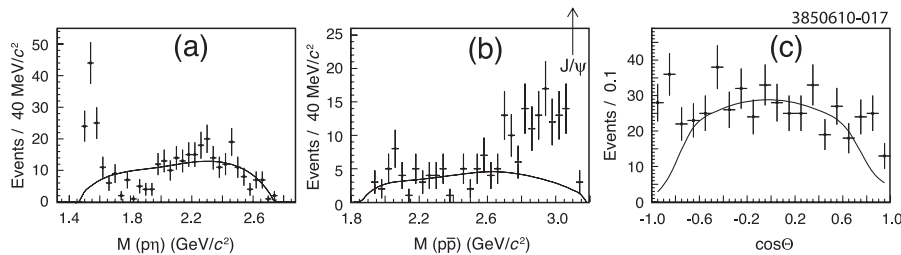

FIG. 17. Distributions in data (points) compared to the phase space MC distributions: (a) the $M(p\eta)$ distributions; (b) the $M(p\bar{p})$ invariant mass distributions; (c) the $\cos\Theta$ distributions. Normalization of the curves is arbitrary in all plots.

TABLE V. Fractions and efficiencies for the intermediate resonances for the best fits for the reaction $\psi(2S) \to \eta p\bar{p}$.

Resonance	M (MeV/c^2)	Γ (MeV/c^2)	Fraction (%)	ϵ
$N^*(1535)$	1535 ± 10	150 ± 25	80 ± 6	0.294
$R_1(2100)$	2103 ± 8	209 ± 19	20 ± 6	0.259

In the $M(p\eta)$ invariant mass distribution [Fig. 17(a)] no evidence is found for $N_1^*(1440)$ and $N_2^*(2300)$ resonances seen in the $M(p\pi^0)$ plot of Fig. 15(a), but a large peak is observed at $M(p\eta) \sim 1540$ MeV/c^2. This suggests excitation of $N^*(1535)$ $J^P = \frac{1}{2}^-$ nucleon resonance of PDG08 [13] with $M = 1525$–1545 (MeV/c^2) and $\Gamma =$ 125–175 (MeV/c^2), which is known to decay into $N\eta$ with a branching fraction of (45–60)%.

In the $M(p\bar{p})$ distribution [Fig. 17(b)] there is a broad enhancement in the 2.7–3.0 GeV/c^2 region which arises mainly as reflection of the $N^*(1535)$ resonance in $M(p\eta)$. In addition there is a narrow enhancement near $M(p\bar{p}) \approx$ 2100 MeV/c^2 reminiscent of the one observed in $M(p\bar{p})$ from $\psi(2S) \to \pi^0 p\bar{p}$ decay.

The optimized masses and widths we obtain for these resonances, and their fractions and estimated efficiencies, are shown in Table V. It is found that the MC-determined efficiencies are insensitive to the uncertainties in masses and widths of the resonances.

We fit our data distribution for $M(p\eta)$ and $M(p\bar{p})$ with an admixture of MC simulated shapes for these two resonances (the fit result shows that the contribution from the phase space MC is consistent with zero). The best fit admixture is

$$(0.20 \pm 0.06) \times R_1(2100) + (0.80 \pm 0.06) \times N^*(1535). \tag{11}$$

The final results for the $M(p\eta)$, $M(p\bar{p})$, and $\cos\Theta$ distributions are presented in Fig. 18 with solid lines. The dashed and dotted lines represent the contributions from the individual resonances. Good agreement between the data and the fitted distributions is obtained for all three distributions, with χ^2/d.o.f. are 35/30 ($M(p\eta)$), 30/30 ($M(p\bar{p})$), and 32/20 ($\cos\Theta$).

The $M^2(p\eta)$ versus $M^2(\bar{p}\eta)$ Dalitz plot in Fig. 16(c) constructed with the MC distributions for the above resonance admixture is seen to reproduce very well the Dalitz plot of data in Fig. 16(b).

Determination of $\mathcal{B}(\psi(2S) \to \eta p\bar{p})$

We consider the entire $M(p\bar{p})$ spectrum with $M(p\bar{p}) <$ 3.077 GeV/c^2 in Fig. 18(b) for the determination of $\mathcal{B}(\psi(2S) \to \eta p\bar{p})$.

We obtain $N = 184 \pm 14$ $\psi(2S) \to \eta p\bar{p}$ candidate events. We do not find any background contribution from feed-down from other decay channels. We estimate the continuum contribution of $\eta p\bar{p}$ production by using the data taken at $\sqrt{s} = 3.67$ GeV. It leads to the luminosity-normalized contribution $N_{\text{cont}} = 30 \pm 8$ counts.

The reconstruction efficiencies determined from the $R_1(2100)$ and $N^*(1535)$ MC simulations are 25.9% and 29.4%, respectively, and the overall effective efficiency of the resonances admixture is $\langle\epsilon\rangle = (28.7 \pm 0.2)\%$.

This yields a branching fraction of

$$\mathcal{B}(\psi(2S) \to \eta p\bar{p}) = \frac{N - N_{\text{cont}}}{\langle\epsilon\rangle \times N_{\psi(2S)} \times \mathcal{B}(\eta \to \gamma\gamma)}$$
$$= (5.6 \pm 0.6(\text{stat})) \times 10^{-5}. \tag{12}$$

This is in agreement with the PDG08 [13] value of $(6.0 \pm 1.2) \times 10^{-5}$, and has a factor 2 smaller error. We can determine the product branching ratios for the production of $N^*(1535)$ and $R_1(2100)$ resonances by taking account of their respective fractions and efficiencies. We obtain

$$\mathcal{B}(\psi(2S) \to \bar{p}N^*(1535)) \times \mathcal{B}(N^*(1535) \to p\eta)$$
$$= (4.4 \pm 0.6(\text{stat})) \times 10^{-5}, \tag{13}$$

$$\mathcal{B}(\psi(2S) \to \eta R_1(2100)) \times \mathcal{B}(R_1(2100) \to p\bar{p})$$
$$= (1.2 \pm 0.4(\text{stat})) \times 10^{-5}. \tag{14}$$

These are the first determinations of these product branching fractions. Estimates of systematic errors are provided in Sec. IX.
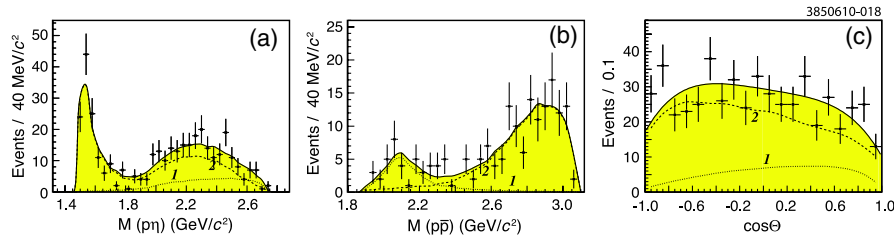

FIG. 18 (color online). Distributions in data (points) compared to the sum of the MC distributions in the proportions given in Table V (solid lines): (a) the $M(p\eta)$ distributions; (b) the $M(p\bar{p})$ distributions; (c) the $\cos\Theta$ distributions. The individual contributions are $R_1(2100)$ shown with the dotted line marked 1, $N^*(1535)$ shown with the dashed line marked 2.

VIII. SEARCH FOR $p\bar{p}$ THRESHOLD ENHANCEMENT IN $J/\psi \to \gamma p \bar{p}$

Although the number of $\pi^+\pi^-$ tagged J/ψ events in our sample of $\psi(2S) \to \pi^+\pi^- J/\psi$ is 8.7×10^6, as compared to the 58×10^6 event J/ψ sample of BES II, it is instructive to analyze it for the subthreshold resonance with $M(p\bar{p}) = 1859^{+3+5}_{-10-25}$ MeV/c^2 reported by BES [5].

For selection of $\psi(2S) \to \pi^+\pi^- J/\psi$, $J/\psi \to \gamma p\bar{p}$ events, we require first $\chi^2_{p\bar{p}\text{vertex}} < 20$ and $\chi^2_{\text{fit}}/\text{d.o.f.} < 3$ of the J/ψ mass constrained fit to $p\bar{p}$ and most energetic shower in the event, then $\chi^2_{\text{vertex}} < 40$ and $\chi^2_{\text{fit}}/\text{d.o.f.} < 10$ of the four-momentum conservation constrained fit to $\pi^+\pi^-$ and J/ψ.

In Fig. 19 we show the distribution of $p\bar{p}$ invariant mass as a function of $\Delta M = M(p\bar{p}) - 2m_p$ in the extended mass region $\Delta M = 0$–970 MeV/c^2. We believe that it is essential to analyze the data in the extended mass region, because as we have seen for $\psi(2S)$ decays, higher mass resonances make contributions all the way down to the $p\bar{p}$ threshold. Further, as shown in Fig. 19, a much better estimate of the phase space contribution can be made when data in the extended mass region are taken into account. Figure 19 shows an enhancement near the $p\bar{p}$ threshold and a large broad enhancement around $\Delta M \approx 200$ MeV/c^2. We therefore analyze our data in the extended mass region, $\Delta M = 0$–970 MeV/c^2, and take account of possible resonances other than the one near the $p\bar{p}$ threshold. Our analysis differs in this essential respect from that of BES in which data in the limited region, $\Delta M = 0$–300 MeV/c^2, was analyzed, and no account was taken of the enhancement around $\Delta M \approx 200$ MeV/c^2.

We have made an attempt to fit the present ΔM distribution with a threshold resonance plus the complement of resonances and phase space observed in the case of $\psi(2S) \to \gamma p\bar{p}$, i.e., $f_2(1950)$ (corresponding to $\Delta M \approx 74$ MeV/c^2), $f_2(2150)$ (corresponding to $\Delta M \approx 224$ MeV/c^2), and phase space. No evidence for a
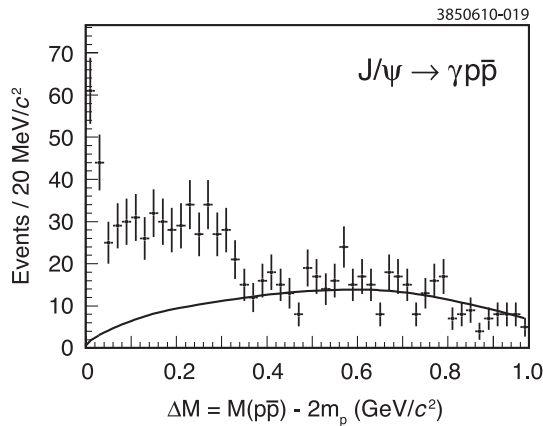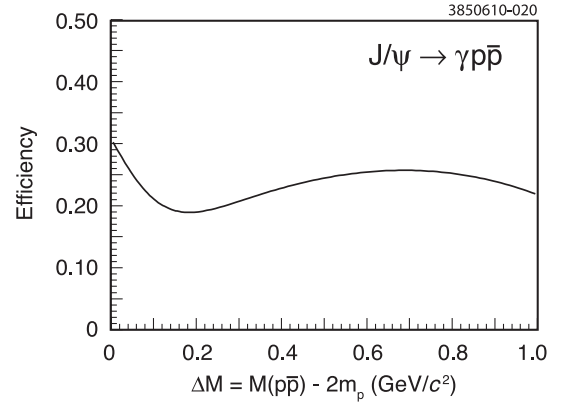

FIG. 20. MC-determined efficiency as a function of $\Delta M \equiv M(p\bar{p}) - 2m_p$ for $J/\psi \to p\bar{p}$ decays. The weighted average efficiency over the whole range is 25.4%.

contribution due to the $f_2(1950)$ resonance was found. All subsequent fits were therefore tried with an S-wave threshold resonance plus MC shapes determined for contributions of a resonance at $M = 2100 \pm 20$ (MeV/c^2), $\Gamma = 160 \pm 20$ (MeV/c^2) (our optimum values), and phase space. The MC-determined event selection efficiency as a function of
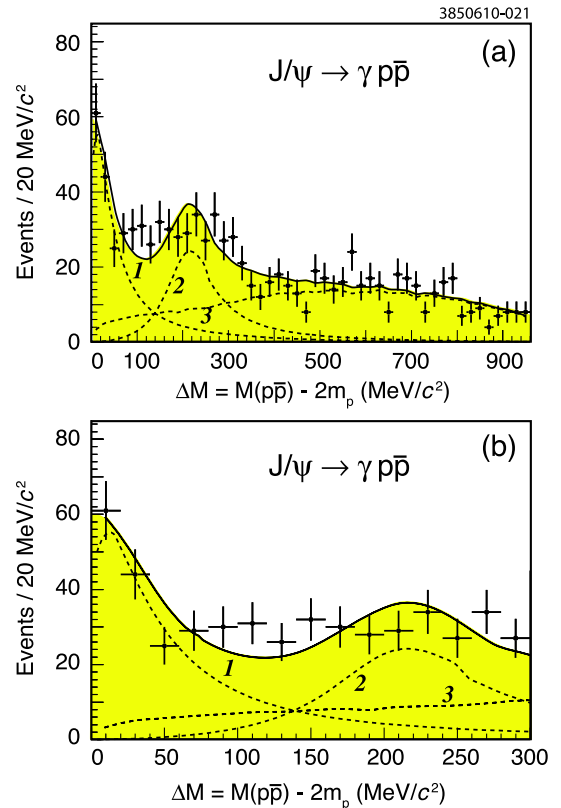

FIG. 21 (color online). Fits of the $\Delta M = M(p\bar{p}) - 2m_p$ invariant mass distribution for $J/\psi \to \gamma p\bar{p}$ decays. Dashed lines are the contributions of (1) R_{thr}, (2) $f_2(2100)$, and (3) the phase space. The solid line is the sum of all three contributions. (a) Fit in the full region $\Delta M = 0$–970 MeV/c^2. (b) Same fit in the $\Delta M = 0$–300 MeV/c^2.

FIG. 19. The $\Delta M = M(p\bar{p}) - 2m_p$ invariant mass distribution for the data for $J/\psi \to \gamma p\bar{p}$. The curve illustrates the shape of the phase space contribution.

ΔM is shown in Fig. 20. The average efficiency, weighted by the threshold resonance contribution, as shown by the curves marked (1) in Fig. 21, was found to be $\epsilon = 0.254$.

We find that if, like BES, we fit the ΔM distribution only in the region $\Delta M = 0$–300 MeV/c^2, and do not consider the contribution due to the resonance at $M(p\bar{p}) = 2100$ MeV/c^2, we obtain a good fit (χ^2/d.o.f. $= 15/26$) which is essentially identical to that obtained by BES [5], with the results

$$M(R_{\text{thr}}) = 1861^{+16}_{-6} \text{ MeV}/c^2,$$

$$\Gamma(R_{\text{thr}}) = 0^{+32}_{-0} \text{ MeV}/c^2,$$

$$\mathcal{B}(J/\psi \to \gamma R_{\text{thr}}) \times \mathcal{B}(R_{\text{thr}} \to p\bar{p}) = (5.9^{+2.8}_{-3.2}) \times 10^{-5}. \quad (15)$$

The errors are statistical only.

Fitting data in the extended region $\Delta M = 0$–970 MeV/c^2 leads to a better determination of the phase space contribution; it is smaller than what is obtained if the fit is confined to the small region, $\Delta M = 0$–300 MeV/c^2. The fit with all parameters kept free (χ^2/d.o.f. $= 97/89$) leads to the fractional contributions of $f_2(2100)$ of $(22 \pm 3)\%$ and phase space $(54 \pm 3)\%$. The threshold resonance obtains 231^{+85}_{-59} counts and leads to the following parameters:

$$M(R_{\text{thr}}) = 1837^{+10+9}_{-12-7} \text{ MeV}/c^2,$$

$$\Gamma(R_{\text{thr}}) = 0^{+44}_{-0} \text{ MeV}/c^2,$$

$$\mathcal{B}(J/\psi \to \gamma R_{\text{thr}}) \times \mathcal{B}(R_{\text{thr}} \to p\bar{p}) = (11.4^{+4.3+4.2}_{-3.0-2.6}) \times 10^{-5}. \quad (16)$$

The first errors are statistical, and the second errors are estimates of systematic errors obtained by varying the mass and width of the 2100 MeV/c^2 resonance by their 1σ uncertainties. The same result, $M(R_{\text{thr}}) = 1837^{+9}_{-12}$ MeV/c^2, is obtained when $\Gamma(R_{\text{thr}})$ is fixed to 20 MeV/c^2.

Figure 21(a) shows the fit in the region $\Delta M = 0$–970 MeV/c^2, and Fig. 21(b) shows the same fit in the $\Delta M = 0$–300 MeV/c^2 region.

The fit result for mass in Eq. (16) is consistent with the conjecture that the threshold enhancement might be due to the tail of a subthreshold resonance at that mass. This possibility was raised earlier by BES with its observation of a resonance with mass $M(R) = 1833.7 \pm 6.1 \pm 2.7$ MeV/c^2 in the reaction $J/\psi \to \gamma R$, $R \to \pi^+ \pi^- \eta$ [18].

IX. SYSTEMATIC UNCERTAINTIES

In Table VI we list various contributions to the systematic uncertainties in the branching fractions. References to

TABLE VI. Sources of systematic uncertainties in branching fractions in %. References to previous CLEO publications for estimates of uncertainties are given in square brackets.

Source	Reference	$\gamma p \bar{p}$	$\pi^0 p \bar{p}$	$\eta p \bar{p}$
Number of $\psi(2S)$	[19]	2.0	2.0	2.0
Trigger efficiency	[20,21]	1.0	1.0	1.0
Tracking efficiency	[22]	2×1.0	2×1.0	2×1.0
Particle identification	[19]	1.0	1.0	1.0
γ, π^0, η reconstruction	[21]	1.0	2.0	4.0
Background subtraction		1.0	1.4	2.0
Subtotal (quadrature)		3.5	4.0	5.5
Resonance fractions		2.4	0.8	0.7
Total (quadrature)		4.2	4.1	5.5

TABLE VII. Summary of the measured quantities. First errors are statistical, and second errors are systematic.

Quantity	Events	Our result (10^{-5})	PDG08 (10^{-5})
$\mathcal{B}(\psi(2S) \to \gamma p \bar{p})$	348 ± 22	$4.18 \pm 0.26 \pm 0.18$	2.9 ± 0.6
$\mathcal{B}(\psi(2S) \to \pi^0 p \bar{p})$	948 ± 37	$15.4 \pm 0.6 \pm 0.6$	13.3 ± 1.7
$\mathcal{B}(\psi(2S) \to \eta p \bar{p})$	154 ± 16	$5.6 \pm 0.6 \pm 0.3$	6.0 ± 1.2
$\mathcal{B}(\psi(2S) \to \gamma f_2(1950)) \times \mathcal{B}(f_2(1950) \to p \bar{p})$	111 ± 19	$1.2 \pm 0.2 \pm 0.1$	
$\mathcal{B}(\psi(2S) \to \gamma f_2(2150)) \times \mathcal{B}(f_2(2150) \to p \bar{p})$	73 ± 18	$0.72 \pm 0.18 \pm 0.03$	
$\mathcal{B}(\psi(2S) \to \bar{p} N_1^*(1440)) \times \mathcal{B}(N_1^*(1440) \to p \pi^0)$	474 ± 42	$8.1 \pm 0.7 \pm 0.3$	
$\mathcal{B}(\psi(2S) \to \bar{p} N_2^*(2300)) \times \mathcal{B}(N_2^*(2300) \to p \pi^0)$	265 ± 39	$4.0 \pm 0.6 \pm 0.2$	
$\mathcal{B}(\psi(2S) \to \pi^0 R_1(2100)) \times \mathcal{B}(R_1(2100) \to p \bar{p})$	76 ± 29	$1.1 \pm 0.4 \pm 0.1$	
$\mathcal{B}(\psi(2S) \to \pi^0 R_2(2900)) \times \mathcal{B}(R_2(2900) \to p \bar{p})$	133 ± 38	$2.3 \pm 0.7 \pm 0.1$	
$\mathcal{B}(\psi(2S) \to \bar{p} N^*(1535)) \times \mathcal{B}(N^*(1535) \to p \eta)$	123 ± 16	$4.4 \pm 0.6 \pm 0.3$	
$\mathcal{B}(\psi(2S) \to \eta R_1(2100)) \times \mathcal{B}(R_1(2100) \to p \bar{p})$	31 ± 10	$1.2 \pm 0.4 \pm 0.1$	

previous CLEO studies for several of these are also given. The uncertainty in feed-down and continuum contributions to the background leads to systematic uncertainties of 1%, 1.4%, and 2% in $\gamma p \bar{p}$, $\pi^0 p \bar{p}$, and $\eta p \bar{p}$, respectively. All the above contributions add in quadrature to 3.5%, 4.0%, and 5.5% uncertainty in $\gamma p \bar{p}$, $\pi^0 p \bar{p}$, and $\eta p \bar{p}$, respectively. Since the uncertainties in the fractions of individual resonance and continuum contributions are taken into account in the statistical uncertainties, the above are the systematic uncertainties in the product branching fractions for the individual resonances in these decays. For $\mathcal{B}(\psi(2S) \rightarrow \gamma p \bar{p})$, $\mathcal{B}(\psi(2S) \rightarrow \pi^0 p \bar{p})$, and $\mathcal{B}(\psi(2S) \rightarrow \eta p \bar{p})$, the uncertainties in the fractions of individual resonance and continuum contributions lead to additional systematic uncertainties because the different contributions have different efficiencies. To take account of correlations in the fractions, the effective overall efficiencies were determined by MC simulations and the relative uncertainties found to be 2.4%, 0.8%, and 0.7% for $\gamma p \bar{p}$, $\pi^0 p \bar{p}$, and $\eta p \bar{p}$, respectively. Thus the total systematic uncertainties in $\mathcal{B}(\psi(2S) \rightarrow \gamma p \bar{p})$, $\mathcal{B}(\psi(2S) \rightarrow \pi^0 p \bar{p})$, and $\mathcal{B}(\psi(2S) \rightarrow \eta p \bar{p})$ are 4.2%, 4.1%, and 5.5%, respectively.

The results for the branching fractions with systematic errors are given in Table VII.

It is found that ± 100 MeV/c^2 changes in the masses and widths of resonances introduce changes in branching fractions much less than 1%.

X. SUMMARY AND CONCLUSIONS

Using CLEO data for 24.5×10^6 $\psi(2S)$ we have studied decays $\psi(2S) \rightarrow \gamma p \bar{p}$, $\pi^0 p \bar{p}$, and $\eta p \bar{p}$. In all three decays we find that intermediate $N^*(\bar{N}^*)$ states decaying into $\pi^0 N(\bar{N})$ and $\eta N(\bar{N})$, and f_J, a_J meson resonances decaying into $p \bar{p}$, make important contributions to the total decay. We have determined branching fractions for the total decay and for the contributions of the individual intermediate states. For the total decays our branching fractions have factors 2 to 3 smaller uncertainties than in the current literature. The product branching fractions for decays through individual intermediate states have been determined for the first time. The results are summarized in Table VII.

We do not find any evidence for a threshold enhancement in any of the three $\psi(2S)$ decay channels. For $\psi(2S) \rightarrow \gamma p \bar{p}$ we set a stringent upper limit for the threshold resonance R_{thr}, $\mathcal{B}(\psi(2S) \rightarrow \gamma R_{\text{thr}}) \times \mathcal{B}(R_{\text{thr}} \rightarrow p \bar{p}) < 1.6 \times 10^{-6}$ at 90% CL.

With a limited sample of 8.6×10^6 J/ψ available to us from $\psi(2S) \rightarrow \pi^+ \pi^- J/\psi$ we have searched for $J/\psi \rightarrow \gamma R_{\text{thr}}$. We find a $p \bar{p}$ threshold enhancement. When it is analyzed taking into account an enhancement at $M(p \bar{p}) = 2100$ MeV/c^2, we obtain $M(R_{\text{thr}}) = 1837^{+10+9}_{-12-7}$MeV/$c^2$, $\Gamma(R_{\text{thr}}) = 0^{+44}_{-0}$MeV/$c^2$, and $\mathcal{B}(J/\psi \rightarrow \gamma R_{\text{thr}}) \times \mathcal{B}(R_{\text{thr}} \rightarrow p \bar{p}) = (11.4^{+4.3+4.2}_{-3.0-2.6}) \times 10^{-5}$.

ACKNOWLEDGMENTS

[1] J.-M. Richard, Nucl. Phys. B, Proc. Suppl. **86**, 361 (2000).

[2] A. Antonelli *et al.*, Nucl. Phys. **B517**, 3 (1998).

[3] K. Abe *et al.* (Belle Collaboration), Phys. Rev. Lett. **88**, 181803 (2002).

[4] K. Abe *et al.* (Belle Collaboration), Phys. Rev. Lett. **89**, 151802 (2002).

[5] J. Z. Bai *et al.* (BES Collaboration), Phys. Rev. Lett. **91**, 022001 (2003).

[6] M.-Z. Wang *et al.* (Belle Collaboration), Phys. Rev. Lett. **92**, 131801 (2004); Phys. Lett. B **617**, 141 (2005).

[7] B. Aubert *et al.* (*BABAR* Collaboration), Phys. Rev. D **72**, 051101 (2005).

[8] B. Aubert *et al.* (*BABAR* Collaboration), Phys. Rev. D **74**, 051101 (2006).

[9] J.-T. Wei *et al.* (Belle Collaboration), Phys. Lett. B **659**, 80 (2008).

[10] For a review of various suggestions see A. Sibirtsev *et al.*, Phys. Rev. D **71**, 054010 (2005), and references therein.

[11] R. A. Briere *et al.* (CLEO-c/CESR-c Taskforces and CLEO-c Collaboration), Cornell University LEPP Report No. CLNS 01/1742, 2001 (unpublished); Y. Kubota *et al.*, Nucl. Instrum. Methods Phys. Res., Sect. A **320**, 66 (1992); D. Peterson *et al.*, Nucl. Instrum. Methods Phys. Res., Sect. A **478**, 142 (2002); M. Artuso *et al.*, Nucl. Instrum. Methods Phys. Res., Sect. A **554**, 147 (2005).

[12] T. Sjöstrand *et al.*, Comput. Phys. Commun. **135**, 238 (2001).

[13] C. Amsler *et al.* (Particle Data Group), Phys. Lett. B **667**, 1 (2008).

[14] M. Ablikim *et al.* (BES Collaboration), Phys. Rev. Lett. **99**, 011802 (2007).

[15] M. Ablikim *et al.* (BES Collaboration), Phys. Rev. D **71**, 072006 (2005).

[16] S. B. Athar *et al.* (CLEO Collaboration), Phys. Rev. D **70**, 112002 (2004).

[17] P. Naik *et al.* (CLEO Collaboration), Phys. Rev. D **78**, 031101(R) (2008).

[18] M. Ablikim *et al.* (BES Collaboration), Phys. Rev. Lett. **95**, 262001 (2005).

[19] S. B. Athar *et al.* (CLEO Collaboration), Phys. Rev. D **70**, 112002 (2004).

[20] T. K. Pedlar *et al.* (CLEO Collaboration), Phys. Rev. D **72**, 051108(R) (2005).

[21] N. E. Adam *et al.* (CLEO Collaboration), Phys. Rev. Lett. **94**, 012005 (2005).

[22] Q. He *et al.* (CLEO Collaboration), Phys. Rev. Lett. **95**, 121801 (2005).